

Generative Adversarial Networks

Gilad Cohen and Raja Giryes

Abstract Generative Adversarial Networks (GANs) are very popular frameworks for generating high-quality data, and are immensely used in both the academia and industry in many domains. Arguably, their most substantial impact has been in the area of computer vision, where they achieve state-of-the-art image generation. This chapter gives an introduction to GANs, by discussing their principle mechanism and presenting some of their inherent problems during training and evaluation. We focus on these three issues: (1) mode collapse, (2) vanishing gradients, and (3) generation of low-quality images. We then list some architecture-variant and loss-variant GANs that remedy the above challenges. Lastly, we present two utilization examples of GANs for real-world applications: Data augmentation and face images generation.

1 Introduction to GANs

Generative adversarial networks (GANs) are currently the leading method to learn a distribution of a given dataset and generate new examples from it. To begin to understand the concept of GANs, let us consider an interplay between the police and money counterfeiters. A state just launched its new currency and millions of bills and coins are widespread all over the country. Recently, the police detected a flood of counterfeit money in circulation. Further inspection reveals that the forged bills are lighter than the genuine bills, and can be easily filtered out. The criminals then find out about the police's discovery and use new printers which control better the cash weight. In turn, the police investigate and discover that the new counterfeit bills have a different texture near the corners, and remove them from the system. After many iterations of generating and discriminating forged money, the counterfeit

Gilad Cohen
Tel Aviv University, Tel Aviv 6997801, e-mail: giladco1@post.tau.ac.il

Raja Giryes
Tel Aviv University, Tel Aviv 6997801 e-mail: raja@tauex.tau.ac.il

money becomes almost indistinguishable from the real money. Note that the system has two agents: 1) The counterfeiters who create "close to real" money and 2) The police who detect counterfeit bills adequately.

Back to deep learning: The above two agents are called "generator" and "discriminator", respectively. These two entities are trained jointly, where the generator learns how to fool the discriminator with new adversarial examples out of the dataset distribution; and the discriminator learns to distinguish between real and fake data samples. The GAN architecture is used in more and more applications since its introduction in 2014. It was proved successful in many domains such as computer vision [14, 29, 25, 38], semantic segmentation [39, 27, 70, 24], time-series synthesis [9, 23], image editing [61, 36, 19, 3, 75], natural language processing [15, 28, 22], text-to-image generation [59, 58, 54], and many more. In the next section, we depict the basic GAN architecture and loss. Later, we will present more sophisticated architectures, losses, and common usages.

2 The basic GAN concept

The first GAN that was introduced by Goodfellow et al. [20] is depicted in Fig. 1.

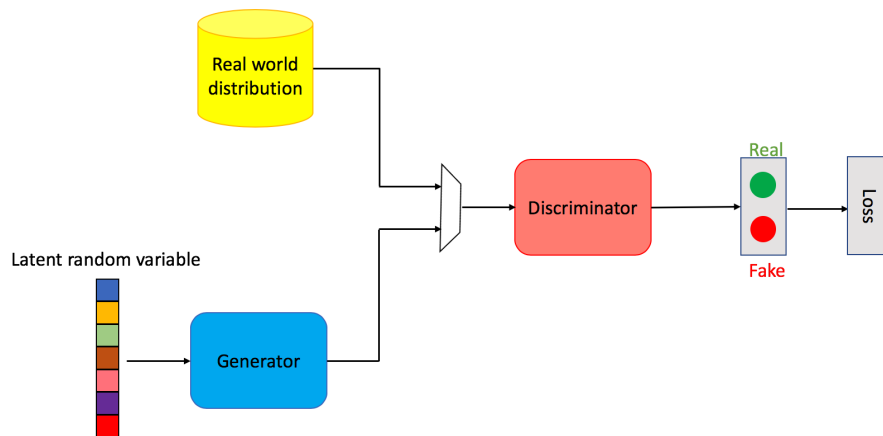


Fig. 1 Basic GAN structure. The discriminator and generator are two deep neural networks trained jointly. The discriminator is trained for the task of classifying whether an input image is natural (real) or generated (fake), while the generator is optimized to fool the discriminator.

The architecture of GANs is comprised from two individual components: A discriminator (D) and a generator (G). D is trained to distinguish between real images from the natural distribution and generated images, while G is trained to craft fake images which fool the discriminator. A random distribution, $\mathbf{z} \sim p_{\mathbf{z}}$, is given as input to G . The purpose of GANs is to learn the generated samples'

distribution, $G(\mathbf{z}) \sim p_g$ that estimates the real world distribution p_r . GANs are optimized by solving the following min-max optimization problem:

$$\min_G \max_D \mathbb{E}_{\mathbf{x} \sim p_r} \log[D(\mathbf{x})] + \mathbb{E}_{\mathbf{z} \sim p_z} \log[1 - D(G(\mathbf{z}))]. \quad (1)$$

On the one hand, D aims at predicting $D(\mathbf{x}) = 1$ for real data samples and $D(G(\mathbf{z})) = 0$ for fake samples. On the other hand, the GAN learns how to fool D by finding G which is optimized on hampering the second term in Eq. (1).

On the first iteration, only the discriminator weights θ_D are updated. We sample a minibatch of m noise samples $\{\mathbf{z}^{(1)}, \dots, \mathbf{z}^{(m)}\}$ from p_z and a minibatch of m real data examples $\{\mathbf{x}^{(1)}, \dots, \mathbf{x}^{(m)}\}$ from p_r . We then calculate the discriminator's gradients

$$\nabla_{\theta_D} \frac{1}{m} \sum_{i=1}^m \left[\log D(\mathbf{x}^{(i)}) + \log(1 - D(G(\mathbf{z}^{(i)}))) \right],$$

and update the discriminator weights, θ_D , by ascending this term. On the second iteration, only the generator's weights θ_G are updated. We sample a minibatch of m noise samples $\{\mathbf{z}^{(1)}, \dots, \mathbf{z}^{(m)}\}$ from p_z , and calculate the generator's gradients

$$\nabla_{\theta_G} \frac{1}{m} \sum_{i=1}^m \log(1 - D(G(\mathbf{z}^{(i)}))), \quad (2)$$

and update the generator weights, θ_G , by descending this term. Goodfellow et al. [20] showed that under certain conditions on D , G , and the training procedure, the distribution p_z converges to p_r .

3 GAN Advantages and Problems

Since their first introduction in 2014, GANs have attracted a growing interest all over the academia and industry, thanks to many advantages over other generative models (mainly Variational Auto-encoders (VAEs) [34]):

- **Sharp images:** GANs produce sharper images than other generative models. The images at the output of the Generator look more natural and with better quality than images generated using VAEs, which tend to be blurrier.
- **Configurable size:** The latent random variable size is not restricted, enriching the generator search space.
- **Versatile generator:** The GAN framework can support many different generator networks, unlike other generative models that may have architectural constraints. VAEs, for example, enforce using a Gaussian at the generator's first layer.

The above advantages make GANs very attractive in the deep learning community, achieving state-of-the-art results in a variety of domains, and generating very natural

images. Yet, the original GAN suffers from three major problems that are described in detail below. We first present a short summary of them:

- **Mode collapse:** During the synchronized training of the generator and discriminator, the generator tends to learn to produce a specific pattern (mode) which fools the discriminator. Although this pattern minimizes Eq. (1), the generator does not cover the full distribution of the dataset.
- **Vanishing gradients:** Very frequently the discriminator is trained "too well" to distinguish real images from adversarial images; in this scenario, the training step of the generator back propagates very low gradients, which does not help the generator to learn.
- **Instability:** The model (θ_D or θ_G) parameters fluctuate, and generally not stable during the training. The generator seldom achieves a point where it outputs very high-quality images.

3.1 Mode collapse

Data distributions are multi-modal, meaning that every sample is classified (usually) to only one label. For example, in MNIST there are ten classes of digits (or modes) labeled from '0' to '9'. Mode collapse is the phenomenon where the generator only yields a small subset of the possible modes. In Fig. 2 you can observe generated MNIST images by two different GANs. The top row shows the training of a "good" GAN, not suffering from mode collapse. It generates every kind of mode (digit type) throughout the training. The bottom row exhibits a GAN training with mode collapse, generating just the digit '6'.

3.2 Vanishing gradients

GANs often suffer from training instability, where D performs very well and G does not get a chance to train a good distribution. We turn to provide some mathematical observations and understanding of why training a generator G is extremely hard when the discriminator D is close to optimal.

The global optimality, stated in [20], is defined when D is optimized for any given G . The optimal D is achieved when its derivative for Eq. (1) equals 0:

$$\begin{aligned} \frac{p_r(\mathbf{x})}{D(\mathbf{x})} - \frac{p_g(\mathbf{x})}{1 - D(\mathbf{x})} &= 0, \\ D^*(\mathbf{x}) &= \frac{p_r(\mathbf{x})}{p_r(\mathbf{x}) + p_g(\mathbf{x})}, \end{aligned} \tag{3}$$

where \mathbf{x} is the real input data, $D^*(\mathbf{x})$ is the optimal discriminator, and $p_r(\mathbf{x})/p_g(\mathbf{x})$ is the distribution of the real/generated data, respectively, over the real data \mathbf{x} . If we

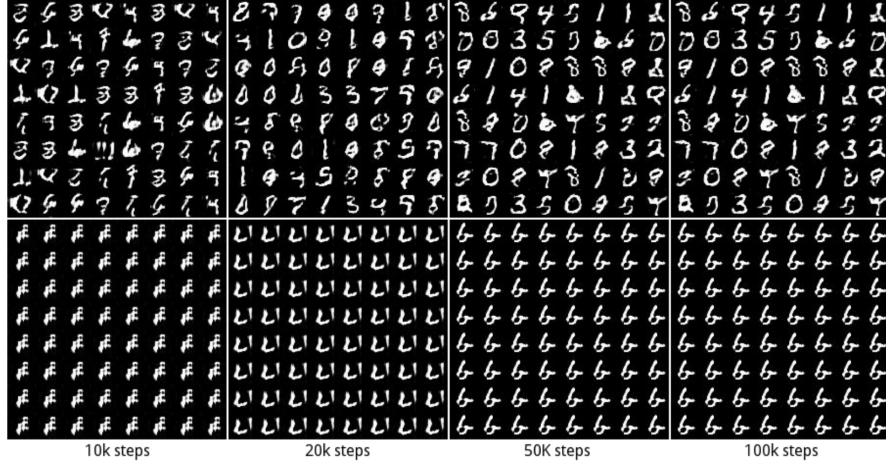


Fig. 2 Example of the mode collapse problem in GANs. The top row shows a training without mode collapse, where all MNIST modes (digits) are generated. The bottom row shows a bad training with mode collapse, where the generator outputs only the digit '6'. Figure was taken from [44].

substitute the optimal discriminator $D^*(\mathbf{x})$ into Eq. (1), we can visualize the loss for the generator G :

$$\mathbb{L}_G = \mathbb{E}_{\mathbf{x} \sim p_r} \log \frac{p_r(\mathbf{x})}{\frac{1}{2}[p_r(\mathbf{x}) + p_g(\mathbf{x})]} + \mathbb{E}_{\mathbf{x} \sim p_g} \log \frac{p_g(\mathbf{x})}{\frac{1}{2}[p_r(\mathbf{x}) + p_g(\mathbf{x})]} - 2 \cdot \log 2. \quad (4)$$

Before we continue any further, we mention two important metrics for probability measurement. The first one is the Kullback-Leiblar (KL) divergence:

$$KL(p_1 || p_2) = \mathbb{E}_{\mathbf{x} \sim p_1} \log \frac{p_1}{p_2}, \quad (5)$$

which measures how much the distribution p_2 differs from the distribution p_1 . Note that this metric is not symmetrical, i.e., $KL(p_1 || p_2) \neq KL(p_2 || p_1)$. A symmetrical metric is Jensen-Shannon (JS) divergence, defined as:

$$JS(p_1 || p_2) = \frac{1}{2} KL(p_1 || \frac{p_1 + p_2}{2}) + \frac{1}{2} KL(p_2 || \frac{p_1 + p_2}{2}). \quad (6)$$

Back to our GAN with the optimal D , Eq. (4) shows that the GAN loss function can be reformulated as:

$$\mathbb{L}_G = 2 \cdot JS(p_r || p_g) - 2 \cdot \log 2, \quad (7)$$

which shows that for D^* , the generator loss turns to be a minimization of the JS divergence between p_r and p_g . The relation between GAN training and the JS divergence may explain its instability. To understand this, view Fig. 3, which shows

an example for JS divergences of different distributions. In Fig. 3(a) we see the real image distribution p_r , as a Gaussian with zero mean, and we consider three examples for generated image distributions: p_{g1} , p_{g2} , and p_{g3} . Fig. 3(b) plots the $JS(p_r(\mathbf{x}), p_q(\mathbf{x}))$ measure between p_r and some p_q distribution, where the mean of p_q ranges from 0 to 80. As shown in the red box, the gradient of the JS divergence vanishes after a mean of 30. In other words, when the discriminator is close to optimal ($D^*(\mathbf{x})$), and we try to train a "poor" generator with p_g far from the real distribution p_r , training will not be feasible due to extremely low gradients. This is prominent especially in the beginning of the training where G weights are randomized.

Due to the vanishing gradient problem, Goodfellow *et al.* [20] proposed a change to the original adversarial loss. Instead of minimizing $\log(1 - D(G(\mathbf{z})))$ (as in Eq. (2)), they suggest to maximize $\log(D(G(\mathbf{z})))$. The latter cost function yields the same fixed point of D and G dynamics but maintains higher gradients early in the training when the distributions p_r and p_g are far from each other. On the other hand, this training strategy promotes mode collapse, as we show next.

With an optimal discriminator D^* , $KL(p_g||p_r)$ can be reformulated as:

$$\begin{aligned} KL(p_g||p_r) &= \mathbb{E}_{\mathbf{x} \sim p_g} \log \frac{p_g(x)/(p_r(x) + p_g(x))}{p_r(x)/(p_r(x) + p_g(x))}, \\ &= \mathbb{E}_{\mathbf{x} \sim p_g} \log \frac{1 - D^*(x)}{D^*(x)}, \\ &= \mathbb{E}_{\mathbf{x} \sim p_g} \log[1 - D^*(x)] - \mathbb{E}_{\mathbf{x} \sim p_g} \log[D^*(x)]. \end{aligned} \quad (8)$$

If we switch the order of the two sides in Eq. (8), we get:

$$\begin{aligned} -\mathbb{E}_{\mathbf{x} \sim p_g} \log[D^*(x)] &= KL(p_g||p_r) - \mathbb{E}_{\mathbf{x} \sim p_g} \log[1 - D^*(x)], \\ &= KL(p_g||p_r) - 2 \cdot JS(p_r||p_g) + 2 \cdot \log 2 + \mathbb{E}_{\mathbf{x} \sim p_r} \log[D^*(x)]. \end{aligned} \quad (9)$$

The alternative loss for G is thus only affected by the first two terms (the last two terms are constant). Since $JS(p_r||p_g)$ is bounded by $[0, \log 2]$ (see Fig. 3(b)), the loss function is dominated by $KL(p_g||p_r)$, which is also called the reverse KL divergence. since $KL(p_g||p_r)$ usually does not equal $KL(p_r||p_g)$, the optimized p_g by the reversed KL is totally different than p_g optimized by the KL divergence. Fig. 4 shows the difference of the two optimization where the distribution p is a mixture of two Gaussians, and q is a single Gaussian. When we optimize for $KL(p_r||p_g)$, q averages all of p modes to hit the mass center (Fig. 4(a)). However, for the reverse KL divergence optimization, q distribution chooses a single mode (Fig. 4(b)), which will cause a mode collapse during training.

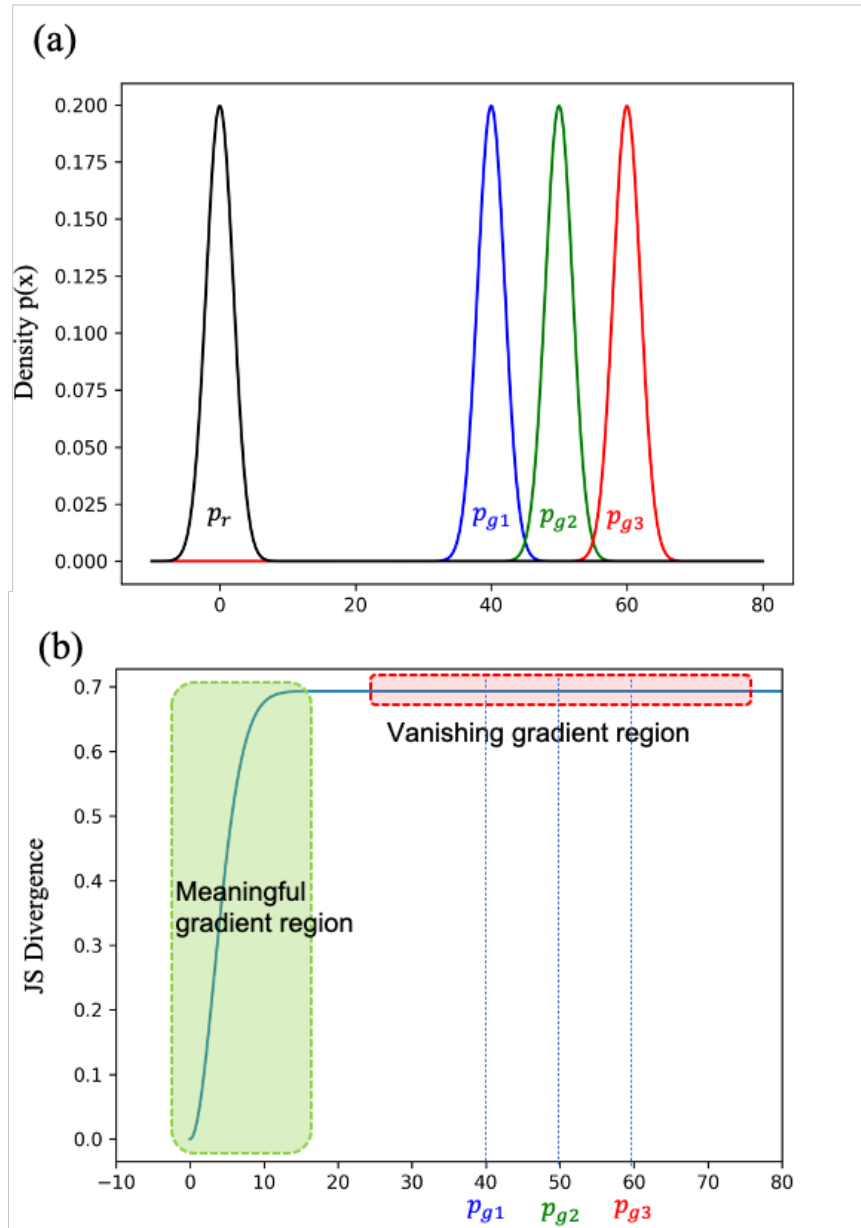


Fig. 3 Vanishing gradients in GANs. (a) An example of a real image distribution $p_r(\mathbf{x})$, a Gaussian with zero mean, with three more different Gaussian distributions: p_{g1} , p_{g2} , and p_{g3} . (b) Calculating the JS divergence measure between $p_r(\mathbf{x})$ and a Gaussian distribution with mean from 0 to 80. When training with optimal discriminator ($D^*(\mathbf{x})$), the generator G minimizes the loss in Eq. (6), pushing $p_g(\mathbf{x})$ left towards $p_r(\mathbf{x})$, alas, it could take a very long time due to diminished gradients when being far from $p_r(\mathbf{x})$.

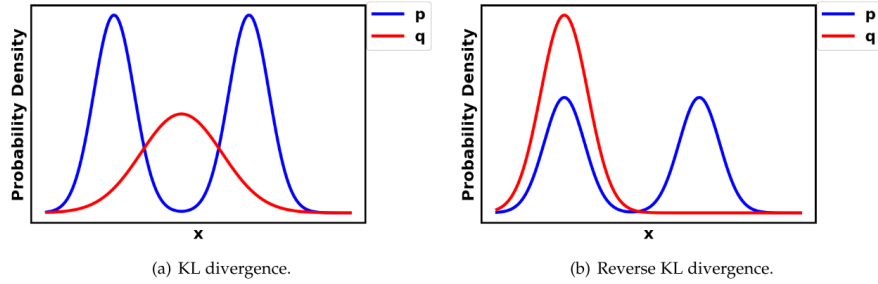


Fig. 4 Optimized distribution q for (a) minimizing KL divergence $KL(p||q)$ and for (b) minimizing reverse KL divergence $KL(q||p)$. Figure is taken from [71].

In summary, using the original G loss from Eq. (1) will result in vanishing gradients for G , and using the other loss in Eq. (9) will result in a mode collapse. These problems are inherent within the GAN loss and thus cannot be solved using sophisticated architectures. In Section 5 we discuss other loss functions for GANs, which solve these problems.

3.3 Instability and Image quality

Early GAN models which use the G losses described above $(\log(1 - D(G(\mathbf{z})))$ and $-\log(D(G(\mathbf{z})))$) exhibit great instability in their cost values during training. Arjovsky *et al.* [4] experimented with these two G losses and claimed that in both cases the gradients cause instability to the GAN training. The loss in Eq. (1) stays constant after the first training steps (Fig. 5(a)), and the loss in Eq. (8) fluctuates during the entire training (Fig. 5(b)). In both cases, they did not find a significant correlation between the calculated loss and the generated image quality. In other words, it is very difficult to predict when during the training the generator actually produces good quality images, and the only way to get a good generator is to stop the training and manually visualize many generated images.

Using the above two G losses in Eq. (1) and Eq. (8) yield poor quality images compared to modern GAN models. In the following sections we will cover more sophisticated losses that enhance the generator’s resolution and image size.

3.4 Problems: summary

The original GAN model and loss proposed by Goodfellow *et al.* [20] suffer from three inherent challenges: (1) Mode collapse; (2) Vanishing gradients; and (3) Image quality. Follow-up works improve the performance of GANs on one or more of these

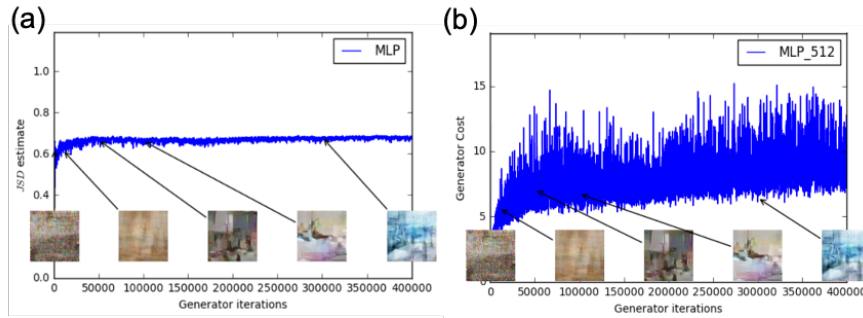


Fig. 5 Training instability in GANs. (a) JS distance metric in GAN training using the loss in Eq. (1). This quantity correlates poorly to the generated image quality, saturating to $\log 2 \approx 0.69$, the highest value taken by the JS distance. (b) Generator loss during training using a different generator cost (maximizing $\log(D(G(\mathbf{z})))$ instead of minimizing $\log(1 - D(G(\mathbf{z})))$) showing increasing error without a significant improvement in image quality. Plots are taken from [4]

problems by using different architectures for D or G , modifying the cost function, and more. A subset of architecture-variant and loss-variant GANs are portrayed in Fig. 6(a),(b), respectively. A sample of some recent prominent GAN models are presented in the following sections.

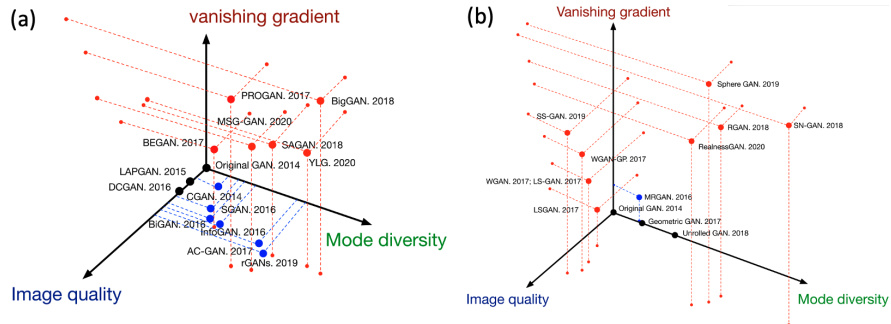


Fig. 6 Recent GAN models which solve the original GAN's problems: Mode diversity (collapse), vanishing gradients, and image quality. (a) A subset of architecture-variant GANs, (b): A subset of loss-variant GANs. Larger axis values indicate better performance. Red points indicate the model improves all three challenges, blue points improve two, and black points improve only one. Figures are taken from [72].

4 Improved GAN architectures

Many types of new GAN architectures have been proposed since 2014 ([6, 8, 13, 29, 57, 77, 30, 16]). Different GAN architectures were proposed for different tasks, such as image super-resolution [38] and image-to-image transfer [79, 53]. In this section we present some of these models, which improved the performance on image quality, vanishing gradients, and mode collapse, compared to the original GAN.

4.1 Semi-supervised GAN (SGAN)

Semi-supervised learning is a promising research field between supervised learning and unsupervised learning. In supervised learning, each data is labeled, and in unsupervised learning, no labels are provided; Semi-supervised learning has labels only for a small subset of the training data, and no annotations for the rest of the data, like many real-world problems.

SGAN [49] extended the original GAN learning to the semi-supervised context by adding to the discriminator network an additional task of classifying the image labels (Fig. 7). The generator's architecture is the same as before. In SGAN the discriminator utilizes two heads, a softmax and a sigmoid. The sigmoid is used to distinguish between real and fake images, and the softmax predicts the images' labels (only for images predicted as real). The results on MNIST showed that both D and G in SGAN are improved compared to the original GAN.

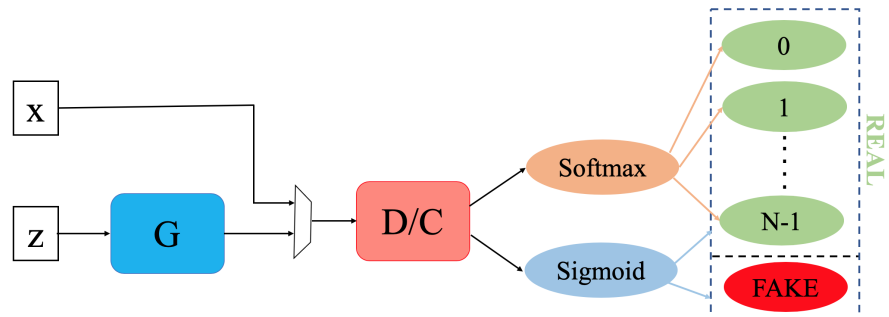


Fig. 7 SGAN architecture.

4.2 Conditional GAN (CGAN)

CGAN was originally proposed as an extension of the original GAN, where both the discriminator and generator were fed by an additional class of the image [45, 50]. An

illustration of CGAN architecture is shown in Fig. 8. In this setup the loss function in Eq. (1) is slightly modified to condition both the real images x and the latent variable z on y (the label):

$$\min_G \max_D \mathbb{E}_{x \sim p_r} \log[D(x|y)] + \mathbb{E}_{z \sim p_z} \log[1 - D(G(z|y))]. \quad (10)$$

All values (x, y, z) are first encoded by some neural layers prior to their fusion in the discriminator and generator. This improves the ability of the discriminator to classify real/fake images and enhances the generator's ability to control the modalities of the generated images. [45] showed that their CGAN architecture used with a language model can handle also multimodal datasets, such as Flickr that contains labeled image data with their particular user tags. They demonstrated that their generator is capable of producing an automatic tagging.

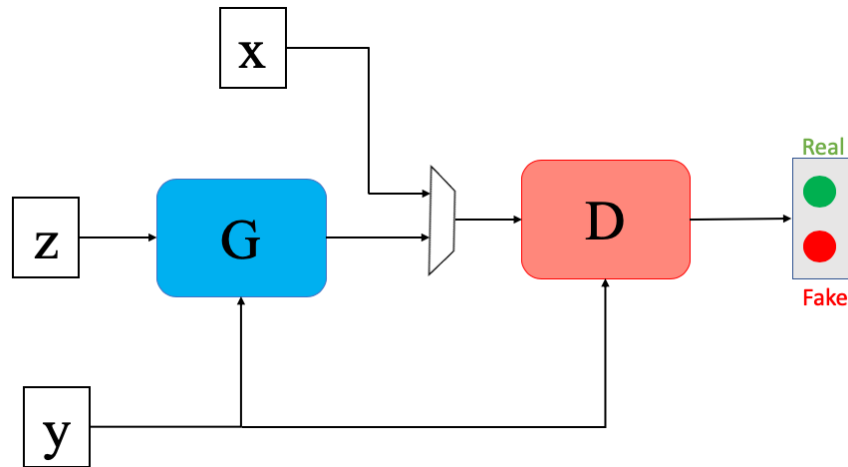


Fig. 8 CGAN architecture. Both the generator and discriminator are fed with a class label y to condition both the images x and latent variable z (see Eq. (10)).

4.3 Deep Convolutional GAN (DCGAN)

Before describing DCGAN, we provide a brief reminder of what is a convolutional neural network.

CNNs: Convolutional neural networks (CNNs) were proposed by LeCun *et al.* [37]; These networks consist of trained spatial filters applied on hidden activations throughout their architecture. These networks perform correlations using their trained kernels with a sliding window over images (or hidden activations).

This was shown to improve the accuracy on many recognition tasks, especially in computer vision. A very basic and popular CNN network called LeNet is shown in Fig. 9.

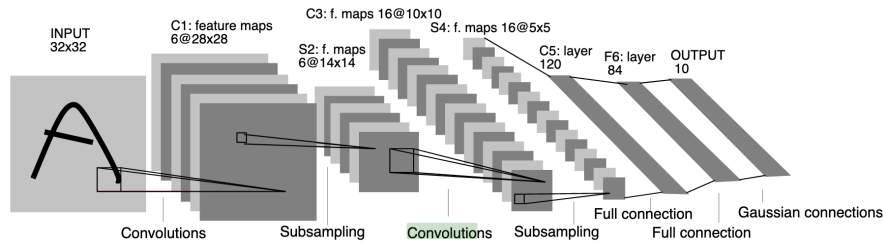


Fig. 9 LeNet architecture. A popular Convolutional Neural Network (CNN) used for image recognition. Image was taken from [37].

DCGAN proposed to create images using solely deconvolutional networks in their generator [57]. The generator architecture is depicted in Fig. 10. Deconvolutional networks can be conceived as CNNs that use the same components but in reverse, projecting features into the image pixel space. [76] showed that deconvolutional layers achieve good visualization for CNNs; this allowed the DCGAN generator to create high-resolution images for the first time.

In addition to improved resolution, DCGAN showed better stability during the training thanks to multiple modifications in the original GAN network:

- All pooling layers were replaced. In the discriminator, they used convolution kernels with stride > 1 , and the generator utilized fractional-strided convolution to increase the spatial size.
- Both the discriminator and generator were trained with batch normalization which promotes similar statistics for real images and fake generated images.
- The discriminator architecture replaces all normal ReLU activations with Leaky-ReLU [40]; this activation multiplies also the negative kernel output by a small value (0.2), to prevent from "dead" gradients to propagate to the generator. The generator architecture used ReLU after every deconvolution layer except the output, which uses Tanh activation.

The authors demonstrated empirically that the mere CNN architecture used in DCGAN is not the key contributing factor for the GAN's performance, and the above modifications are crucial. To show that they measured GANs quality by considering them as feature extractors on supervised datasets, and evaluating the performance of linear models trained on these features (for more information see [57]). DCGAN yields a classification error of 22.48% on the StreetView House Numbers dataset (SVHN) [47], whereas a purely supervised CNN with the same architecture achieved a significantly higher 28.87% test error.

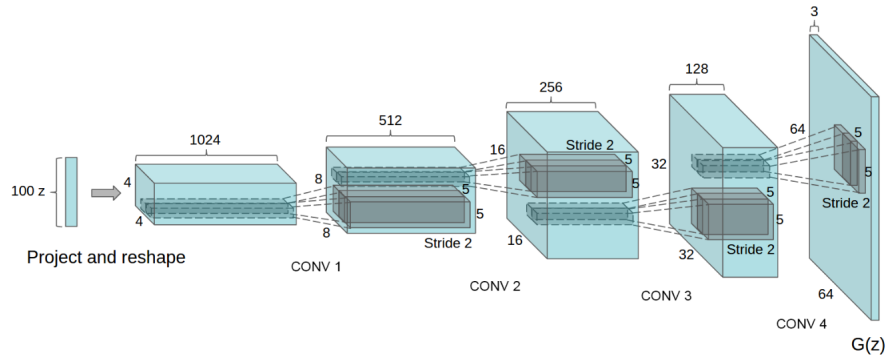


Fig. 10 DCGAN generator architecture. This generator creates a complex 64×64 pixel image from a 100 dimensional uniform distribution z . No fully connected or pooling layers are used. Figure is taken from [57]

4.4 Progressive GAN (PROGAN)

PROGAN described a novel training methodology for GANs, involving progressive steps toward the development of the entire network architecture [29]. This progressive architecture uses the idea of progressive neural networks first proposed by Rusu *et al.* [62]. These architectures are immune to forgetting and can leverage prior knowledge via lateral connections to previously learned features. The progressive training scheme is shown in Fig. 11. First, they trained low resolution 4×4 pixel images. Next, both D and G grow to include a layer of 8×8 spatial resolution. This progressive training gradually adds more and more intermediate layers to enhance the resolution, until reaching a high resolution of 1024×1024 pixel images with the CelebA dataset. All previous layers remain trainable in later steps.

Many state-of-the-art GAN architectures utilize this type of progressive training scheme, and it has resulted in very credible images [29, 30, 8, 32, 60], and more stable learning for both D and G .

4.5 BigGAN

Attention in computer vision is a method that focuses the task on an "interesting" region in the image. The self-attention is used to train the network (usually CNN) in an unsupervised manner, teaching it to segment or localize the most relevant pixels (or activations) for the vision task.

BigGAN [8] has achieved state-of-the-art generation on the ImageNet datasets. Its architecture is based on the Self-attention GAN (SAGAN) [77], which employs a self-attention mechanism in both D and G , to capture a large receptive field without sacrificing computational efficiency for CNNs [69]. The original SAGAN

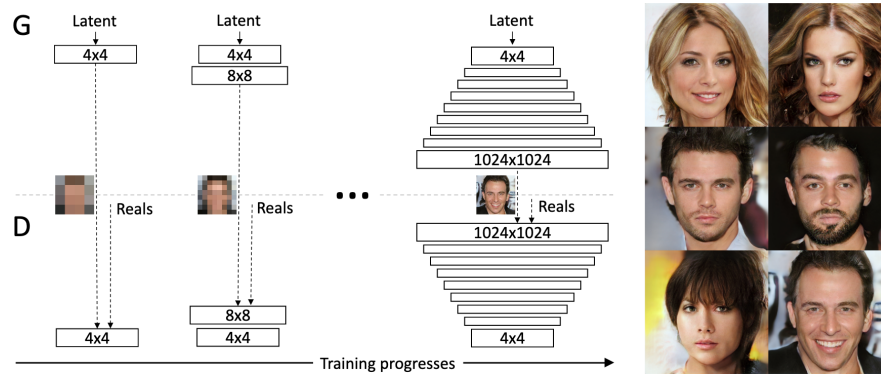


Fig. 11 Training process for the PROGAN progressive methodology. Training starts with both G and D having a low spatial resolution of 4×4 pixels. Every training step adds a new incremented intermediate layer to D and G , enhancing the generated images' resolution. All existing layers are trainable throughout the process. The images on the right are examples of generated images using PROGAN at 1024×1024 . Figure was taken from [29]

architecture can learn global semantics and long-range dependencies for images, thus generating excellent multi-label images based on the ImageNet datasets (128×128 pixels). BigGAN achieved improved performance by scaling up the GAN training: Increasing the number of network parameters ($\times 4$) and increasing the batch size ($\times 8$). They achieved better performance on ImageNet with size 128×128 and were also able to train BigGAN also on the resolutions 256×256 and 512×512 .

Unlike many previous GAN models, which randomized the latent variable from either $z \sim \mathcal{N}(0, 1)$ or $z \sim \mathcal{U}(-1, 1)$, BigGAN uses a simple *truncation trick*. During training z is sampled from $\mathcal{N}(0, 1)$, but for generating images in inference z is selected from a truncated normal, where values that lie outside the range are re-sampled until falling in the range. This *truncation trick* shows improvement in individual sample quality at the cost of a reduction in overall sample variety, as shown in Fig. 12(a). Notice though that using this different inference sampling trick as is may not generate good images with some large models, producing some saturation artifacts (Fig. 12(b)). To solve this issue, the authors proposed to use Orthogonal Regularization to force G to be more amenable to truncation, making it smoother so that the full lateral space will map to good generated images.

4.6 StyleGAN

StyleGAN [30] proposed an alternative generator architecture for GANs. Unlike the traditional G architecture that samples a random latent variable at its input, their architecture starts from a learned constant input and adjust the characteristics of the images in every convolutional layer along G using different, learned latent variables. Additionally, they inject learned noise directly throughout G (see Fig. 13).

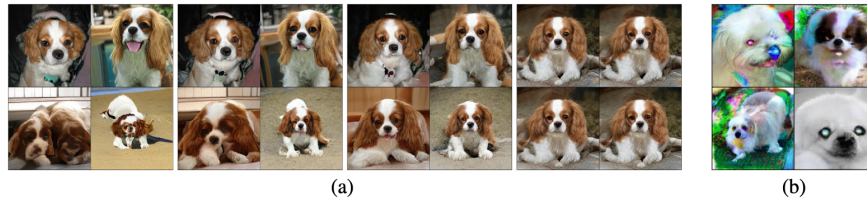


Fig. 12 Using truncated sampling from the latent space. (a) Trade-off between image quality and image variety. From left to right, the range threshold is set to 2, 1, 0.5, and 0.04. (b) Saturation artifacts from applying truncated normal distribution to a model training with $z \sim \mathcal{N}(0, 1)$. Images were taken from [8].

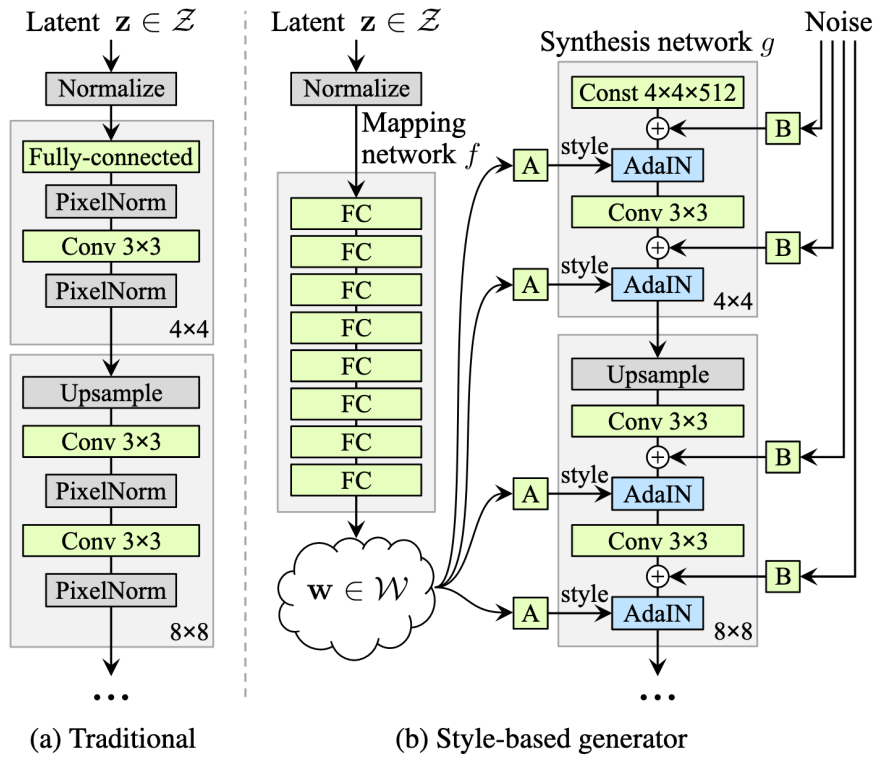


Fig. 13 Comparison between a traditional generator (left) to the StyleGAN generator (right). Unlike the standard generator which selects a random latent variable only in its input, in StyleGAN generator the latent input is mapped to an intermediate latent space \mathcal{W} , which then controls the generator through adaptive instance normalization (AdaIN). Also, Gaussian noise is injected after every convolution layer. "A" corresponds to a learned affine transform, and "B" applies learned scaling factors to the input noise. Figure is taken from [30].

This architectural change leads to automatic, unsupervised separation of high-level attributes (e.g., pose and identity) from low-level variations (e.g., freckles, hair) in the generated images. StyleGAN did not modify the discriminator or the loss function. They used the same D architecture as in [29]. In addition to state-of-the-art quality for face image generation, StyleGAN demonstrates a higher degree of latent space disentanglement, presenting more linear representations of different factors of variation, turning the GAN synthesis to be much more controllable. Recently a more advanced styleGAN architecture has been proposed [32, 18, 33]. Some generated examples are presented in Fig. 14. One may also use StyleGAN for image editing by calculating the latent vector of a given input image in the styleGAN (this operation is known as styleGAN inversion) and then manipulating this vector for editing the image [75, 60, 1, 68, 2, 65, 64, 54].



Fig. 14 Selected face images generated using the StyleGAN2 architecture (an improved version of the original StyleGAN), trained on the FFHQ dataset. Figure from [32].

5 Improved GAN objectives

As described in Section 3.2, the original GAN's min-max loss (Eq. (1)) promotes mode collapse and vanishing gradient phenomena. This section presents selected loss functions and regularizations that remedy these problems and also improves the image quality. This is just a partial list and other loss functions and regularization methods exist such as the least square GANs [41] or optimal transport models [55].

5.1 Wasserstein GAN (WGAN)

WGAN [4] has solved the vanishing gradient and mode collapse problems of the original GAN by replacing the cost in Eq. (1) with the Earth Mover (EM) distance, which is known also as the Wasserstein distance and is defined as:

$$W(p_r, p_g) = \inf_{\gamma \in \Pi(p_r, p_g)} \mathbb{E}_{(x,y) \sim \gamma} [\|x - y\|], \quad (11)$$

where $\Pi(p_r, p_g)$ denotes the set of all joint distributions $\gamma(x, y)$ whose marginals are p_r and p_g , respectively. The EM distance is therefore the minimum cost of transporting "mass" in converting distribution p_r into the distribution p_g .

Unlike KL and JS distances, EM is capable of indicating distance even when the p_r and p_g distributions are far from each other; EM is also continuous and thus provides useful gradients for training G . However, the infimum in Eq. (11) is highly intractable, so the authors estimate the EM cost with:

$$\max_{w \sim \mathcal{W}} \mathbb{E}_{\mathbf{x} \sim p_r} [f_w(\mathbf{x})] - \mathbb{E}_{\mathbf{z} \sim p_z} [f_w(G(\mathbf{z}))], \quad (12)$$

where $\{f_w\}_{w \in \mathcal{W}}$ is a parameterized family of all functions that are K -Lipschitz for some K ($\|f\|_L \leq K$). Readers are referred to [4] for more details.

The authors proposed to find the best function f_w that maximize Eq. (12) by back-propagating $\mathbb{E}_{\mathbf{z} \sim p_z} [\nabla_{\theta} f(g_{\theta}(z))]$, where g_{θ} are the generator's weights. f_w can be realized by D but constrained to be K -Lipschitz and z is the lateral input noise for G . w in f_w are the discriminator's parameters, and the objective of D is to maximize Eq. (12), which approximates the EM distance. When D is optimized, Eq. (12) becomes the EM distance, and G is optimized to minimize it:

$$- \min_G \mathbb{E}_{\mathbf{z} \sim p_z} [f_w(G(\mathbf{z}))] \quad (13)$$

Fig. 15 compares the gradient of WGAN to the original GAN from two non overlapping Gaussian distributions. It can be observed that WGAN has a smooth and measurable gradient everywhere (blue line), and learns better even when G is not producing good images.

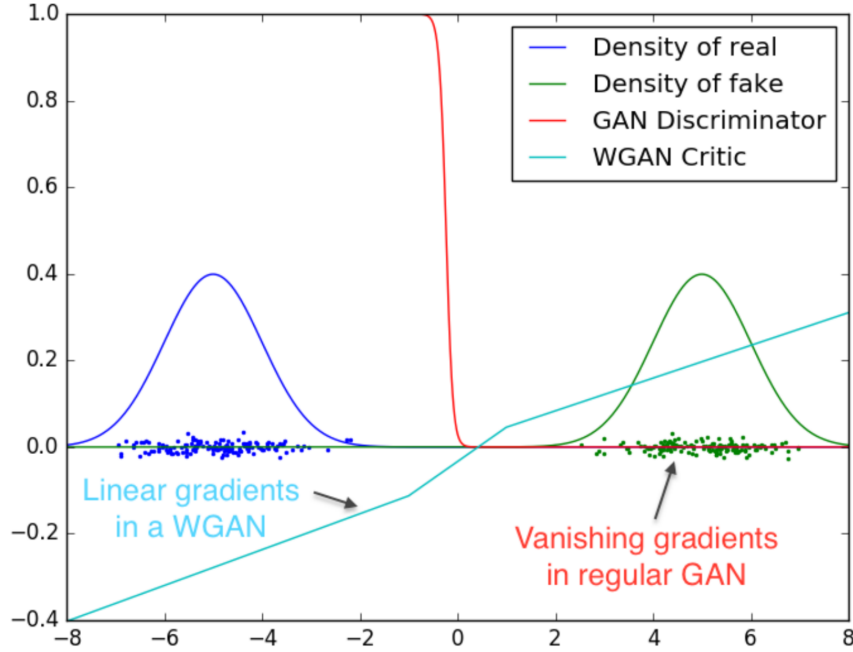


Fig. 15 Differentiating two Gaussian distributions using optimal discriminator D^* . The original GAN cost saturates (red line), resulting in vanishing gradients, whereas WGAN cost objective (blue line) yields measurable gradients. Plot was taken from [4].

5.2 Self Supervised GAN (SSGAN)

We showed in Section 4.2 that CGANs can generate natural images. However, they require labeled images to do so, which is a major drawback. SSGANs [10] exploit two popular unsupervised learning techniques, adversarial training, and self-supervision, bridging the gap between conditional and unconditional GANs.

Neural networks have been shown to forget previous learned tasks [17, 35], and catastrophic forgetting was previously considered as a major cause for GAN training instability. Motivated by the desire to counter the discriminator forgetting, SSGAN adds to the discriminator an additional loss, which enables it to learn useful representations, independently of the quality of the generator. In a self-supervised manner, the authors train a model on a task of prediction a rotation angle ($[0^\circ, 90^\circ, 180^\circ, 270^\circ]$), as shown in Fig. 16. The objectives of D and G are updated to:

$$\begin{aligned} L_G &= -V(G, D) - \alpha \mathbb{E}_{\mathbf{x} \sim P_G} \mathbb{E}_{r \sim \mathbb{R}} [\log Q_D(R = r | \mathbf{x}^r)] \\ L_D &= V(G, D) - \beta \mathbb{E}_{\mathbf{x} \sim P_{data}} \mathbb{E}_{r \sim \mathbb{R}} [\log Q_D(R = r | \mathbf{x}^r)], \end{aligned} \quad (14)$$

where $V(G, D)$ is the original GAN objective in Eq. (1), P_{data} and P_G are the real data and generated data distributions, respectively, $r \in R$ is a rotation selected from

a set of all allowed angles ($R = \{0^\circ, 90^\circ, 180^\circ, 270^\circ\}$). An image \mathbf{x} rotated by r degrees is denoted as \mathbf{x}' , and $Q(R|\mathbf{x}')$ is the discriminator's predictive distribution over the angles of rotation of the sample. These new losses enforce D to learn good representation via learning the rotation information in a self-supervised approach.

Using the above scheme, SSGAN achieves good high-quality images, matching the performance of conditional GANs without having access to labeled data.

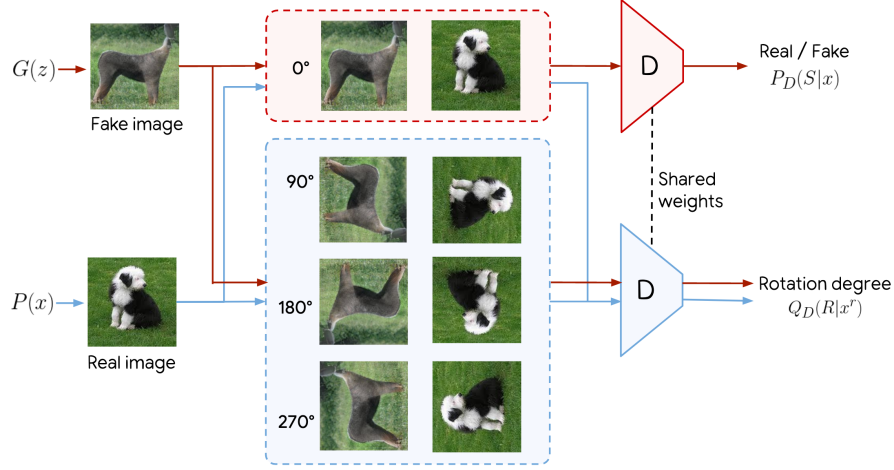


Fig. 16 Self-Supervised GAN (SSGAN) discriminator. The discriminator, D , performs two tasks: Identifying real/fake images (as the original GAN) and rotation classification. Both the real and fake images are rotated by ($[0^\circ, 90^\circ, 180^\circ, 270^\circ]$), and sent to the rotation degree classifier (in blue). Only the original 0° images are sent to the real/fake classifier (in red). Plot is taken from [10].

5.3 Spectral Normalization GAN (SNGAN)

SNGAN [46] proposes to add weight normalization to stabilize the training of the discriminator. Their technique is computationally inexpensive and can be applied easily to existing GANs architectures. In previous works that stabilized GAN training ([21, 4, 56]) it was emphasized that D should be a K -Lipshitz continuous function, forcing it not to change rapidly. This characteristic of D stabilizes the training of GANs. SNGAN controls the Lipschitz constant of D by literally constraining the spectral norm of each layer, normalizing each weight matrix W so it satisfies the spectral constraint $\sigma(W) = 1$ (i.e., the largest singular value of the weight matrix of each layer is 1). This is performed by simply normalizing each layer:

$$\bar{W}_{SN}(W) = \frac{W}{\sigma(W)}, \quad (15)$$

where \mathbf{W} are the weight parameters of each layer in D . This paper proves that this will make the Lipschitz constant of the discriminator function to be bound by 1, which is important for the WGAN optimization.

SNGAN achieves an extraordinary advance on ImageNet, and better or equal quality on CIFAR-10 and STL-10, compared to the previous training stabilization techniques that include weight clipping [4], gradient penalty [74, 43], batch normalization [26], weight normalization [63], layer normalization [5], and orthonormal regularization [7].

5.4 SphereGAN

SphereGAN [52] is a novel integral probability metric (IPM)-based GAN, which uses the hypersphere to bound IPMs in the objective function, thus enhancing the stability of the training. By exploiting the information of higher-order statistics of data using geometric moment matching, they achieved more accurate results. The objective function of SphereGAN is defined as

$$\min_G \max_D \sum_r E_x[d_s^r(\mathbf{N}, D(x))] - \sum_r E_z[d_s^r(\mathbf{N}, D(G(z)))], \quad (16)$$

for $r = 1, \dots, R$ where the function d_s^r measures the r -th moment distance between each sample and the north pole of the hypersphere, \mathbf{N} . Note that the subscript s indicates that d_s^r is defined on \mathbb{S}^n . Fig. 17 shows the pipeline of SphereGAN. By defining IPMs on the hypersphere, SphereGAN can alleviate several constraints that should be imposed on D for stable training, such as the Lipschitz constraints required from conventional discriminators based on the Wasserstein distance.

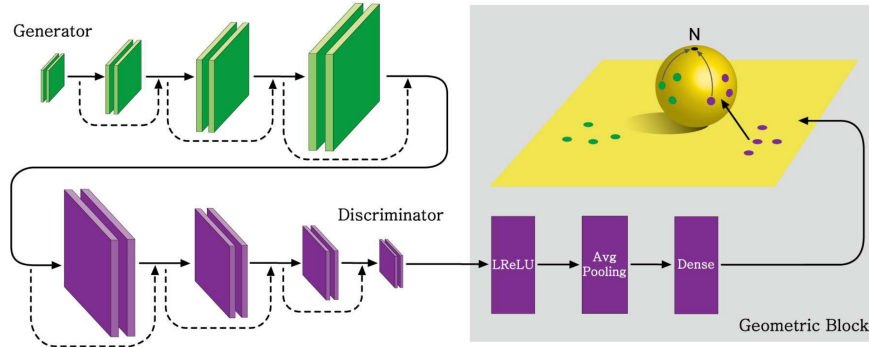


Fig. 17 Pipeline of Sphere GAN. The generator creates fake data from noise inputs. Real and fake data are fed to the discriminator, which maps the output to an n -dimensional Euclidean feature space (yellow plane). Green and purple points on the feature plane correspond to fake and real samples, respectively. The key idea of SphereGAN is remapping the feature points into the n -dimensional hypersphere by using geometric transformations. These mapped points are then used to calculate the geometric moments centered at the north pole of the hypersphere (N). While the discriminator tries to maximize the moment differences of real and fake samples, the generator tries to interfere with the discriminator by minimizing those moment differences. Figure was taken from [52].

Unlike conventional approaches that use the Wasserstein distance and add additional constraint terms (see Table 1 in [52]), SphereGAN does not need any additional constraints to force D in a desired function space, due to the usage of geometric transformation in D .

6 Data augmentation with GAN

We turn now to describe how to use GAN for data augmentation. Data augmentation is a crucial process for tasks lacking large training sets. There are three circumstances which require data augmentation:

- **Limited annotations:** Training a large DNN with a very few labeled data in the training set.
- **Limited diversity:** When the training data lacks variations. For example, it may not cover diverse illuminations or a variety of appearances.
- **Restricted data:** The database might contain sensitive information, and thus accessing it directly is strictly restricted.

The first two scenarios can be solved via supervised learning but they will cost a lot of human effort to enrich the labeled data or to use active learning approaches [11]. An alternative approach is to utilize GANs to augment the data. Semi-supervised GAN (SGAN) (see Section 4.1) is a simple example of such a GAN architecture that is able to generate new annotated images and can automatically enrich training data with few labels.

The second case is more common in the real world. Data variability is important for many psychology or neuroscience experiments. For example, a human's EEG is sensitive to different types of face images such as happy, angry, and sad faces [42]. Preparing those stimuli in traditional experiments is time-consuming and costly for researchers. Architectures like StyleGAN [30] (see Section 4.6) are specialized to generate broad types of face images as a stimulus. More important, these images can be controlled to exhibit specific attributes (e.g. level of happiness or facial textures), and thus enhancing the stimuli variation in the experiment [73]. Data augmentation can be also helpful in the training of the GANs themselves [31, 78], which allows to train them with only few examples and still get high quality generated data (e.g., images).

The last case is related to unsupervised learning approaches. When a database is restricted to preserve users' privacy, researchers can use GANs to synthesize this sensitive data themselves. For example, Delaney *et al.* employed GANs to generate synthetic ECG signals that resemble real ECG data [12].

7 Conclusion

This chapter has provided just a glimpse of GANs and their various usages. This fast-growing technique has many variants and applications that have not been presented here for the sake of brevity. Yet, we believe that the description of GANs given here provides the reader with the tools to better understand this tool and be able to navigate between the vast amount of recent literature on this topic. It is worth mentioning also normalizing flows [51] and score based generative models [67, 66, 48], which become very popular recently and show competitive performance with GANs.

Acknowledgements We would like to thank Yuval Alaluf, Yotam Nitzan and Ron Mokady for their helpful comments.

References

- [1] Rameen Abdal, Yipeng Qin, and Peter Wonka. Image2stylegan: How to embed images into the stylegan latent space? In *2019 IEEE/CVF International Conference on Computer Vision (ICCV)*, pages 4431–4440, 2019.
- [2] Rameen Abdal, Yipeng Qin, and Peter Wonka. Image2stylegan++: How to edit the embedded images? In *Proceedings of the IEEE/CVF Conference on Computer Vision and Pattern Recognition (CVPR)*, June 2020.
- [3] Rameen Abdal, Peihao Zhu, Niloy J. Mitra, and Peter Wonka. Styleflow: Attribute-conditioned exploration of stylegan-generated images using conditional continuous normalizing flows. *ACM Trans. Graph.*, 40(3), May 2021.
- [4] Martin Arjovsky, Soumith Chintala, and Léon Bottou. Wasserstein Generative Adversarial Networks. In *ICML*, volume 70, pages 214–223, 2017.
- [5] Jimmy Lei Ba, Jamie Ryan Kiros, and Geoffrey E. Hinton. Layer Normalization. 7 2016.
- [6] David Berthelot, Tom Schumm, and Luke Metz. {BEGAN:} Boundary Equilibrium Generative Adversarial Networks. *CoRR*, abs/1703.1, 2017.
- [7] Andrew Brock, Theodore Lim, James M Ritchie, and Nick Weston. Neural Photo Editing with Introspective Adversarial Networks. *ArXiv*, abs/1609.0, 2017.
- [8] Andrew Brock, Jeff Donahue, and Karen Simonyan. Large scale GAN training for high fidelity natural image synthesis. In *International Conference on Learning Representations*, 2019.
- [9] Eoin Brophy, Zhengwei Wang, and Tomas E. Ward. Quick and easy time series generation with established image-based gans. *ArXiv*, abs/1902.05624, 2019.
- [10] Ting Chen, Xiaohua Zhai, Marvin Ritter, Mario Lucic, and Neil Houlsby. Self-Supervised GANs via Auxiliary Rotation Loss. *CVPR*, pages 12146–12155, 2019.
- [11] David A Cohn, Zoubin Ghahramani, and Michael I Jordan. Active Learning with Statistical Models. *J. Artif. Int. Res.*, 4(1):129–145, 3 1996. ISSN 1076-9757.
- [12] Anne Marie Delaney, Eoin Brophy, and Tomas E Ward. Synthesis of Realistic ECG using Generative Adversarial Networks. *ArXiv*, abs/1909.0, 2019.
- [13] Emily L Denton, Soumith Chintala, Arthur Szlam, and Robert Fergus. Deep Generative Image Models using a Laplacian Pyramid of Adversarial Networks. *CoRR*, abs/1506.0, 2015.
- [14] Gintare Karolina Dziugaite, Daniel M. Roy, and Zoubin Ghahramani. Training generative neural networks via maximum mean discrepancy optimization. In *Proceedings of the Thirty-First Conference on Uncertainty in Artificial Intelligence*, page 258–267, 2015.

- [15] William Fedus, Ian Goodfellow, and Andrew M. Dai. MaskGAN: Better text generation via filling in the $_$. In *International Conference on Learning Representations*, 2018.
- [16] Yuri Feigin, Hedva Spitzer, and Raja Giryes. Generative adversarial encoder learning, 2020.
- [17] Robert M French. Catastrophic forgetting in connectionist networks. *Trends in Cognitive Sciences*, 3(4):128–135, 1999.
- [18] Rinon Gal, Dana Cohen Hochberg, Amit Bermano, and Daniel Cohen-Or. Swagan: A style-based wavelet-driven generative model. *ACM Trans. Graph.*, 40(4), July 2021.
- [19] Rinon Gal, Or Patashnik, Haggai Maron, Gal Chechik, and Daniel Cohen-Or. Stylegan-nada: Clip-guided domain adaptation of image generators, 2021.
- [20] Ian Goodfellow, Jean Pouget-Abadie, Mehdi Mirza, Bing Xu, David Warde-Farley, Sherjil Ozair, Aaron Courville, and Yoshua Bengio. Generative adversarial nets. In *Advances in Neural Information Processing Systems 27*, pages 2672–2680, 2014.
- [21] Ishaan Gulrajani, Faruk Ahmed, Martin Arjovsky, Vincent Dumoulin, and Aaron C Courville. Improved Training of Wasserstein GANs. In *Advances in Neural Information Processing Systems 30*, pages 5767–5777, 2017.
- [22] Jiaxian Guo, Sidi Lu, Han Cai, Weinan Zhang, Yong Yu, and Jun Wang. Long text generation via adversarial training with leaked information. In *Proceedings of the Thirty-Second AAAI Conference on Artificial Intelligence*, pages 5141–5148, 2018.
- [23] Kay Gregor Hartmann, Robin Tibor Schirrmeyer, and Tonio Ball. Eeg-gan: Generative adversarial networks for electroencephalographic (eeg) brain signals. *ArXiv*, abs/1806.01875, 2018.
- [24] Judy Hoffman, Eric Tzeng, Taesung Park, Jun-Yan Zhu, Phillip Isola, Kate Saenko, Alexei Efros, and Trevor Darrell. CyCADA: Cycle-consistent adversarial domain adaptation. In *International Conference on Machine Learning*, volume 80, pages 1989–1998, 2018.
- [25] Shady Abu Hussein, Tom Tirer, and Raja Giryes. Image-adaptive gan based reconstruction. In *AAAI*, 2020.
- [26] Sergey Ioffe and Christian Szegedy. Batch Normalization: Accelerating Deep Network Training by Reducing Internal Covariate Shift. In *ICML*, 2015.
- [27] Phillip Isola, Jun-Yan Zhu, Tinghui Zhou, and Alexei A. Efros. Image-to-image translation with conditional adversarial networks. *2017 IEEE Conference on Computer Vision and Pattern Recognition (CVPR)*, pages 5967–5976, 2016.
- [28] Nikolay Jetchev, Urs Bergmann, and Roland Vollgraf. Texture synthesis with spatial generative adversarial networks. *CoRR*, abs/1611.08207, 2016.
- [29] Tero Karras, Timo Aila, Samuli Laine, and Jaakko Lehtinen. Progressive growing of GANs for improved quality, stability, and variation. In *International Conference on Learning Representations*, 2018.
- [30] Tero Karras, Samuli Laine, and Timo Aila. A Style-Based Generator Architecture for Generative Adversarial Networks. *2019 IEEE/CVF Conference on Computer Vision and Pattern Recognition (CVPR)*, pages 4396–4405, 2019.

- [31] Tero Karras, Miika Aittala, Janne Hellsten, Samuli Laine, Jaakko Lehtinen, and Timo Aila. Training generative adversarial networks with limited data. In *Proc. NeurIPS*, 2020.
- [32] Tero Karras, Samuli Laine, Miika Aittala, Janne Hellsten, Jaakko Lehtinen, and Timo Aila. Analyzing and improving the image quality of StyleGAN. In *CVPR*, 2020.
- [33] Tero Karras, Miika Aittala, Samuli Laine, Erik Härkönen, Janne Hellsten, Jaakko Lehtinen, and Timo Aila. Alias-free generative adversarial networks. In *Proc. NeurIPS*, 2021.
- [34] Diederik P Kingma and Max Welling. Auto-encoding variational bayes, 2013.
- [35] James N Kirkpatrick, Razvan Pascanu, Neil C Rabinowitz, Joel Veness, Guillaume Desjardins, Andrei A Rusu, Kieran Milan, John Quan, Tiago Ramalho, Agnieszka Grabska-Barwinska, Demis Hassabis, Claudia Clopath, Dharshan Kumaran, and Raia Hadsell. Overcoming catastrophic forgetting in neural networks. *Proceedings of the National Academy of Sciences*, 114:3521–3526, 2017.
- [36] Guillaume Lample, Neil Zeghidour, Nicolas Usunier, Antoine Bordes, Ludovic DENOYER, et al. Fader networks: Manipulating images by sliding attributes. In *Advances in Neural Information Processing Systems*, pages 5963–5972, 2017.
- [37] Y LeCun, P Haffner, L Bottou, and Yoshua Bengio. Object Recognition with Gradient-Based Learning. In *Shape, Contour and Grouping in Computer Vision*, 1999.
- [38] Christian Ledig, Lucas Theis, Ferenc Huszár, José Antonio Caballero, Andrew Aitken, Alykhan Tejani, Johannes Totz, Zehan Wang, and Wenzhe Shi. Photo-Realistic Single Image Super-Resolution Using a Generative Adversarial Network. *2017 IEEE Conference on Computer Vision and Pattern Recognition (CVPR)*, pages 105–114, 2017.
- [39] Pauline Luc, Camille Couprie, Soumith Chintala, and Jakob Verbeek. Semantic segmentation using adversarial networks. *ArXiv*, abs/1611.08408, 2016.
- [40] Andrew L Maas. Rectifier Nonlinearities Improve Neural Network Acoustic Models. In *ICML*, 2013.
- [41] Xudong Mao, Qing Li, Haoran Xie, Raymond Y.K. Lau, Zhen Wang, and Stephen Paul Smolley. Least squares generative adversarial networks. In *Proceedings of the IEEE International Conference on Computer Vision (ICCV)*, Oct 2017.
- [42] Aimee Mavratzakis, Cornelia Herbert, and Peter Walla. Emotional facial expressions evoke faster orienting responses, but weaker emotional responses at neural and behavioural levels compared to scenes: A simultaneous EEG and facial EMG study. *NeuroImage*, 124:931–946, 2016.
- [43] Lars Mescheder, Sebastian Nowozin, and Andreas Geiger. Which training methods for gans do actually converge? In *International Conference on Machine Learning (ICML)*, 2018.
- [44] Luke Metz, Ben Poole, David Pfau, and Jascha Sohl-Dickstein. Unrolled generative adversarial networks. In *ICLR*, 2017.

- [45] Mehdi Mirza and Simon Osindero. Conditional Generative Adversarial Nets. *ArXiv*, abs/1411.1, 2014.
- [46] Takeru Miyato, Toshiki Kataoka, Masanori Koyama, and Yuichi Yoshida. Spectral Normalization for Generative Adversarial Networks. In *International Conference on Learning Representations*, 2018.
- [47] Yuval Netzer, Tao Wang, Adam Coates, Alessandro Bissacco, Bo Wu, and Andrew Y Ng. Reading Digits in Natural Images with Unsupervised Feature Learning. In *NIPS Workshop on Deep Learning and Unsupervised Feature Learning 2011*, 2011.
- [48] Alexander Quinn Nichol and Prafulla Dhariwal. Improved denoising diffusion probabilistic models. In *International Conference on Machine Learning*, volume 139, pages 8162–8171, 2021.
- [49] Augustus Odena. Semi-Supervised Learning with Generative Adversarial Networks. *ArXiv*, abs/1606.0, 2016.
- [50] Augustus Odena, Christopher Olah, and Jonathon Shlens. Conditional Image Synthesis with Auxiliary Classifier {GAN}s. In *Proceedings of the 34th International Conference on Machine Learning*, volume 70 of *Proceedings of Machine Learning Research*, pages 2642–2651, 2017.
- [51] George Papamakarios, Eric Nalisnick, Danilo Jimenez Rezende, Shakir Mohamed, and Balaji Lakshminarayanan. Normalizing flows for probabilistic modeling and inference. *Journal of Machine Learning Research*, 22(57):1–64, 2021.
- [52] Sung Woo Park and Junseok Kwon. Sphere Generative Adversarial Network Based on Geometric Moment Matching. *2019 IEEE/CVF Conference on Computer Vision and Pattern Recognition (CVPR)*, pages 4287–4296, 2019.
- [53] Taesung Park, Ming-Yu Liu, Ting-Chun Wang, and Jun-Yan Zhu. Semantic image synthesis with spatially-adaptive normalization. In *Proceedings of the IEEE Conference on Computer Vision and Pattern Recognition*, 2019.
- [54] Or Patashnik, Zongze Wu, Eli Shechtman, Daniel Cohen-Or, and Dani Lischinski. Styleclip: Text-driven manipulation of stylegan imagery. In *Proceedings of the IEEE/CVF International Conference on Computer Vision (ICCV)*, pages 2085–2094, October 2021.
- [55] Gabriel Peyre and Marco Cuturi. Computational optimal transport: With applications to data science. *Foundations and Trends® in Machine Learning*, 11(5-6):355–607, 2019.
- [56] Guo-Jun Qi. Loss-Sensitive Generative Adversarial Networks on Lipschitz Densities. *International Journal of Computer Vision*, 128:1118–1140, 2019.
- [57] Alec Radford, Luke Metz, and Soumith Chintala. Unsupervised Representation Learning with Deep Convolutional Generative Adversarial Networks. *CoRR*, abs/1511.0, 2015.
- [58] Alec Radford, Jong Wook Kim, Chris Hallacy, Aditya Ramesh, Gabriel Goh, Sandhini Agarwal, Girish Sastry, Amanda Askell, Pamela Mishkin, Jack Clark, Gretchen Krueger, and Ilya Sutskever. Learning transferable visual models from natural language supervision, 2021.

- [59] Aditya Ramesh, Mikhail Pavlov, Gabriel Goh, Scott Gray, Chelsea Voss, Alec Radford, Mark Chen, and Ilya Sutskever. Zero-shot text-to-image generation, 2021.
- [60] Elad Richardson, Yuval Alaluf, Or Patashnik, Yotam Nitzan, Yaniv Azar, Stav Shapiro, and Daniel Cohen-Or. Encoding in style: a stylegan encoder for image-to-image translation. In *CVPR*, 2021.
- [61] Tamar Rott Shaham, Tali Dekel, and Tomer Michaeli. Singan: Learning a generative model from a single natural image. In *IEEE International Conference on Computer Vision (ICCV)*, 2019.
- [62] Andrei A Rusu, Neil C Rabinowitz, Guillaume Desjardins, Hubert Soyer, James Kirkpatrick, Koray Kavukcuoglu, Razvan Pascanu, and Raia Hadsell. Progressive Neural Networks. *ArXiv*, abs/1606.0, 2016.
- [63] Tim Salimans and Durk P Kingma. Weight Normalization: A Simple Reparameterization to Accelerate Training of Deep Neural Networks. In *Advances in Neural Information Processing Systems 29*, pages 901–909. Curran Associates, Inc., 2016.
- [64] Yujun Shen and Bolei Zhou. Closed-form factorization of latent semantics in gans. In *CVPR*, 2021.
- [65] Yujun Shen, Ceyuan Yang, Xiaoou Tang, and Bolei Zhou. Interfacegan: Interpreting the disentangled face representation learned by gans. *TPAMI*, 2020.
- [66] Jiaming Song, Chenlin Meng, and Stefano Ermon. Denoising diffusion implicit models. In *International Conference on Learning Representations*, 2021. URL <https://openreview.net/forum?id=St1giarCHLP>.
- [67] Yang Song, Jascha Sohl-Dickstein, Diederik P Kingma, Abhishek Kumar, Stefano Ermon, and Ben Poole. Score-based generative modeling through stochastic differential equations. In *International Conference on Learning Representations*, 2021.
- [68] Omer Tov, Yuval Alaluf, Yotam Nitzan, Or Patashnik, and Daniel Cohen-Or. Designing an encoder for stylegan image manipulation. *ACM Trans. Graph.*, 40(4), 2021.
- [69] Ashish Vaswani, Noam Shazeer, Niki Parmar, Jakob Uszkoreit, Llion Jones, Aidan N Gomez, Łukasz Kaiser, and Illia Polosukhin. Attention is All you Need. In *Advances in Neural Information Processing Systems*, pages 5998–6008, 2017.
- [70] T. Wang, M. Liu, J. Zhu, A. Tao, J. Kautz, and B. Catanzaro. High-resolution image synthesis and semantic manipulation with conditional gans. In *IEEE/CVF Conference on Computer Vision and Pattern Recognition*, pages 8798–8807, June 2018. doi: 10.1109/CVPR.2018.00917.
- [71] Zhengwei Wang, Qi She, and Tomas E Ward. Generative Adversarial Networks: {A} Survey and Taxonomy. *CoRR*, abs/1906.0, 2019.
- [72] Zhengwei Wang, Qi She, and Tomas E Ward. Generative Adversarial Networks: {A} Survey and Taxonomy. *CoRR*, abs/1906.0, 2019.
- [73] Zhengwei Wang, Qi She, Alan F Smeaton, Tomás E Ward, and Graham Healy. Synthetic-Neuroscore: Using a neuro-AI interface for evaluating generative adversarial networks. *Neurocomputing*, 405:26–36, 2020.

- [74] Huikai Wu, Shuai Zheng, Junge Zhang, and Kaiqi Huang. GP-GAN: Towards Realistic High-Resolution Image Blending. *Proceedings of the 27th ACM International Conference on Multimedia*, 2019.
- [75] Weihao Xia, Yulun Zhang, Yujiu Yang, Jing-Hao Xue, Bolei Zhou, and Ming-Hsuan Yang. Gan inversion: A survey, 2021.
- [76] Matthew D Zeiler and Rob Fergus. Visualizing and Understanding Convolutional Networks. In *ECCV*, 2014.
- [77] Han Zhang, Ian Goodfellow, Dimitris Metaxas, and Augustus Odena. Self-attention generative adversarial networks. In *International Conference on Machine Learning*, volume 97, pages 7354–7363, 2019.
- [78] Shengyu Zhao, Zhijian Liu, Ji Lin, Jun-Yan Zhu, and Song Han. Differentiable augmentation for data-efficient gan training. In *Conference on Neural Information Processing Systems (NeurIPS)*, 2020.
- [79] Jun-Yan Zhu, Taesung Park, Phillip Isola, and Alexei A Efros. Unpaired Image-to-Image Translation Using Cycle-Consistent Adversarial Networks. *2017 IEEE International Conference on Computer Vision (ICCV)*, pages 2242–2251, 2017.